JACS
JOURNAL OF THE AMERICAN CHEMICAL SOCIETY
pubs.acs.org/JACS
Article

Multiple Proton-Coupled Electron Transfers at a Tricopper Cluster: Modeling the Reductive Regeneration Process in Multicopper Oxidases

Weiyao Zhang, Curtis E. Moore, and Shiyu Zhang*

Cite This: J. Am. Chem. Soc. 2022, 144, 1709−1717
Read Online

ABSTRACT: Metal clusters in enzymes carry out the life-sustaining reactions by accumulating multiple redox equivalents in a narrow potential range. This redox potential leveling effect commonly observed in Nature has yet to be reproduced with synthetic metal clusters. Herein, we employ a fully encapsulated synthetic tricopper complex to model the three-electron two-proton reductive regeneration of fully reduced trinuclear copper cluster $Cu^ICu^ICu^I(\mu_2\text{-}OH_2)$ (**FR**) from native intermediate $Cu^{II}Cu^{II}Cu^{II}(\mu_3\text{-}O)$ (**NI**) in multicopper oxidases (MCOs). The tricopper cluster can access four oxidation states (I,I,I to II,II,II) and four protonation states ($[Cu_3(\mu_3\text{-}O)]$**LH**, $[Cu_3(\mu_3\text{-}OH)]$**L**, $[Cu_3(\mu_3\text{-}OH)]$**LH**, and $[Cu_3(\mu_3\text{-}OH_2)]$**L**, where **LH** denotes the protonated ligand), allowing mechanistic investigation of proton-coupled electron transfer (PCET) relevant to MCOs. Seven tricopper complexes with discrete oxidation and protonation states were characterized with spectroscopy or X-ray single-crystal diffraction. A stepwise electron transfer−proton transfer (ET−PT) mechanism is established for the reduction of $Cu^{II}Cu^{II}Cu^{II}(\mu_3\text{-}O)$**LH** to $Cu^{II}Cu^{II}Cu^{I}(\mu_3\text{-}OH)$**L**, while a stepwise PT−ET mechanism is determined for the reduction of $Cu^{II}Cu^{I}Cu^{I}(\mu_3\text{-}OH)$**LH** to $Cu^{I}Cu^{I}Cu^{I}(\mu_2\text{-}OH_2)$**L**. The switch-over from ET−PT to PT−ET mechanism showcases that the tricopper complex can adopt different PCET mechanisms to circumvent high-barrier proton transfer steps. Overall, three-electron two-proton reduction occurs within a narrow potential range of 170 mV, exemplifying the redox potential leveling effect of secondary proton relays in delivering multiple redox equivalents at metal clusters.

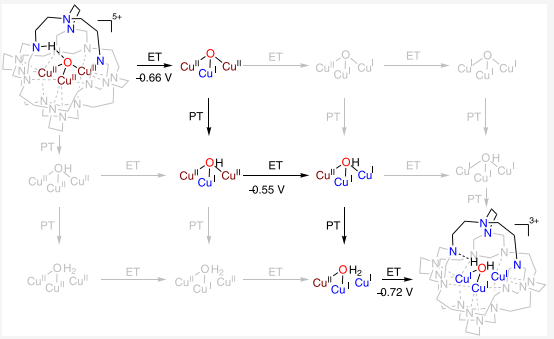

INTRODUCTION

Multielectron transfer is ubiquitous in energy conversion and storage reactions in enzymes, e.g., oxygen reduction,[1] oxygen evolution,[2] CO_2 reduction,[3] and nitrogen fixation.[4] Nature has evolved multimetallic active sites capable of temporary accumulation of multiple redox equivalents before substrate turnover. A salient example is multicopper oxidases (MCOs, Figure 1A), which catalyze the four-electron reduction of O_2 to H_2O, a life-sustaining reaction that is often coupled with the oxidation of various substrates. The trinuclear copper cluster (TNC) gathers three electrons from an adjacent type 1 Cu (T1) electron transfer site (13 Å away) to generate the fully reduced $Cu^ICu^ICu^I$ state (**FR**) before activating O_2 to form the $Cu^{II}Cu^{II}Cu^{II}$ cluster (native intermediate, **NI**, Figure 1B).[1,5−11] Three-electron and three-proton transfer to **NI** regenerates **FR**, completing the catalytic cycle. Considering the mild redox potential of the T1 site (300−800 mV vs NHE),[12] it is remarkable that a single T1 site can deliver three electrons consecutively to the TNC.

Understanding how multi-electron-transfer reactions are performed at metal clusters can provide crucial insights into catalyst design for energy conversion and storage.[13] At present, it is not clear how to construct a synthetic metal cluster that reproduces the function of biological metal clusters in storing multiple redox equivalents in a narrow potential range. For instance, multielectron transfer of synthetic metal clusters typically requires a potential span of 1−2 V (Figure 2A).[14−18] In biological settings, covering such a wide potential range is challenging from both thermodynamic and kinetic perspectives, so Nature often employs proton-coupled electron transfer (PCET) to reduce the potential gap between adjacent redox couples, leveling the redox potential of multielectron transfer.[13,19−21] This "redox potential leveling" effect results from alternating delivery of protons and electrons, which avoids localized charge buildup. Indeed, two carboxylate groups (D94, E487, PDB: 1ZPU) in the secondary coordination sphere of TNC sites have been proposed to serve as a proton relay during regeneration of **FR** from **NI**.[8,9] However, the molecular mechanism by which proton relays

Received: October 16, 2021
Published: January 19, 2022

https://doi.org/10.1021/jacs.1c10948
J. Am. Chem. Soc. 2022, 144, 1709−1717

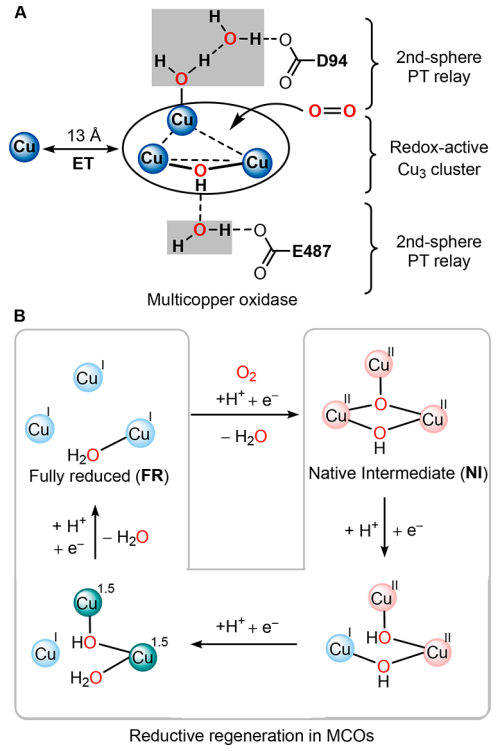

Figure 1. (A) Structural illustration of the active site in MCOs and (B) mechanism of oxygen reduction reaction catalyzed by MCOs. The proposed mechanism for regeneration of **FR** is highlighted with a frame.

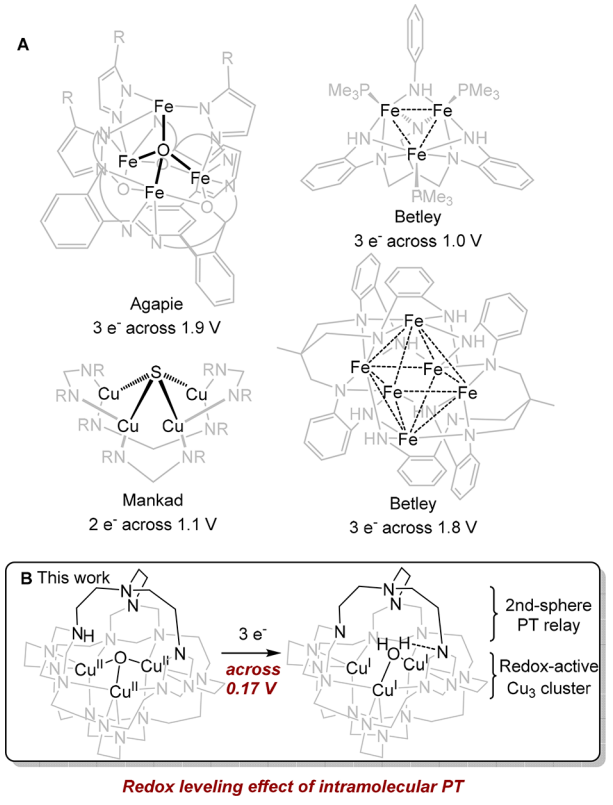

Figure 2. (A) Potential range required for multielectron transfer at redox-active metal clusters in the literature. (B) $3e^-/2H^+$ PCET at the tricopper cluster occurs within a narrow potential range of 170 mV.

assist PCET at the tricopper center is difficult to study.[5,6] Currently, no synthetic models would permit probing of the synergy of a tricopper site with the hydrogen-bonding network in the secondary coordination sphere. It is also challenging to investigate these intricate ET and PT steps with proteins, due to the similar spectroscopic features of ET/PT tricopper intermediates.

Recently, we reported the first tricopper complex that can access all four oxidation states from II,II,II to I,I,I.[22] The tricopper cluster is embedded in a macrocyclic $TREN_4$ (TREN = tris(2-aminoethyl)amine) ligand that provides a rigid coordination environment, leading to lower reorganization energy of electron transfer. The empty TREN motif on top of the tricopper cluster may serve as a pendant proton relay (Figure 2B), mimicking the function of carboxylate groups adjacent to the TNC. The supramolecular construct of $TREN_4$ prevents the pendant proton relay from collapsing into the tricopper center, preserving the cavity as a proton reservoir. Building on this system, we herein demonstrate the three-electron two-proton PCET from $Cu^{II}Cu^{II}Cu^{II}(\mu_3\text{-O})$ to $Cu^{I}Cu^{I}Cu^{I}(\mu_2\text{-}OH_2)$ (Figure 2B). The proton-coupled reduction of II,II,II to I,I,I occurs within a narrow potential range of 170 mV, reflecting the redox potential leveling effect of the pendant proton relay. The synergistic delivery of electron and proton at the tricopper cluster serves as a prototype for multiple proton-coupled electron transfer at multimetallic active sites.

RESULTS AND DISCUSSION

$[TREN_4HCu^{II}Cu^{II}Cu^{II}(\mu_3\text{-O})]^{5+}$ as a Synthetic Model for NI. One-pot reaction of TREN, $[Cu^{I}(MeCN)_4]PF_6$, and paraformaldehyde affords a mixed-valent $[TREN_4Cu^{II}Cu^{I}Cu^{I}(\mu_3\text{-OH})](PF_6)_3$ complex ($Cu^{II}Cu^{I}Cu^{I}(\mu_3\text{-OH})$**L**, **L** denotes the $TREN_4$ ligand).[22] The tricopper μ_3-OH species have been isolated and characterized in I,I,I/II,I,I/II,II,I oxidation states.[22] To prepare a synthetic model for **NI** ($Cu^{II}Cu^{II}Cu^{II}(\mu_3\text{-O})$), we attempted to further oxidize the tricopper cluster to the II,II,II state using two equivalents of oxidant. Treatment of $Cu^{II}Cu^{I}Cu^{I}(\mu_3\text{-OH})$**L** with two equivalents of tris(4-bromophenyl)ammoniumyl hexafluorophosphate (0.67 V vs Fc/Fc^+ in MeCN, Figure 3A) in MeCN resulted in instantaneous bleaching of the dark blue color of ammoniumyl to a yellow solution. The UV−vis spectrum of the tricopper product (Figure S1A), presumably at the II,II,II oxidation state, shows a peak at 690 nm (ε = 1100 M^{-1} cm^{-1}), which is different from that of $Cu^{II}Cu^{II}Cu^{I}(\mu_3$-OH) (850 nm, ε = 1250 M^{-1} cm^{-1}).

Single crystals of the fully oxidized tricopper II,II,II cluster were grown from vapor diffusion of diethyl ether to acetone after partial anion exchange with BF_4^- (see the Supporting Information). The X-ray diffraction analysis reveals a highly symmetric tricopper complex with five positive charges (Figure 3B), suggesting the II,II,II oxidation state. The central ligand could be assigned as either μ_3-OH or μ_3-O (Figure 3A). In the latter case, a proton has been transferred to the top TREN to form $Cu^{II}Cu^{II}Cu^{II}(\mu_3\text{-O})$**LH**, where **LH** denotes a protonated $TREN_4$ ligand. We were unable to crystallographically differentiate the central ligand as μ_3-O or μ_3-OH; therefore, we turn to the spectroscopic characterization of the tricopper complex at the II,II,II state.

In contrast to II,II,I/II,I,I/I,I,I states, the tricopper complex at the II,II,II state does not exhibit a O−H stretch in infrared spectroscopy, suggesting the central ligand is a μ_3-O instead of

https://doi.org/10.1021/jacs.1c10948
J. Am. Chem. Soc. 2022, 144, 1709−1717

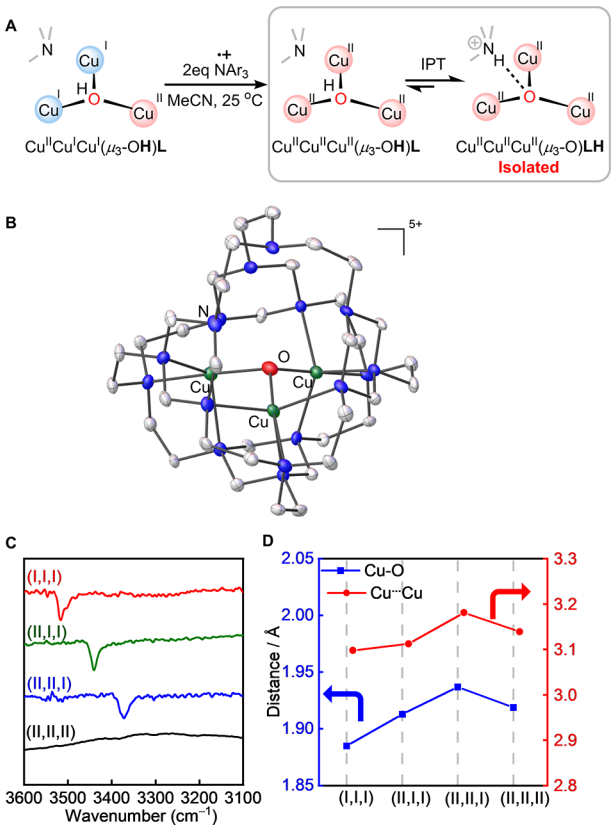

Figure 3. (A) Intramolecular proton transfer at the II,II,II state. (B) Solid-state structure of $(Cu^{II}Cu^{II}Cu^{II}(\mu_3\text{-}O)\mathbf{LH}$. All H atoms, counteranions, and solvent molecules are omitted for clarity. (C) Infrared spectra of tricopper complexes from the I,I,I to II,II,II state. (D) Plot of crystallographically determined Cu−O and Cu···Cu distances as a function of the tricopper oxidation state.

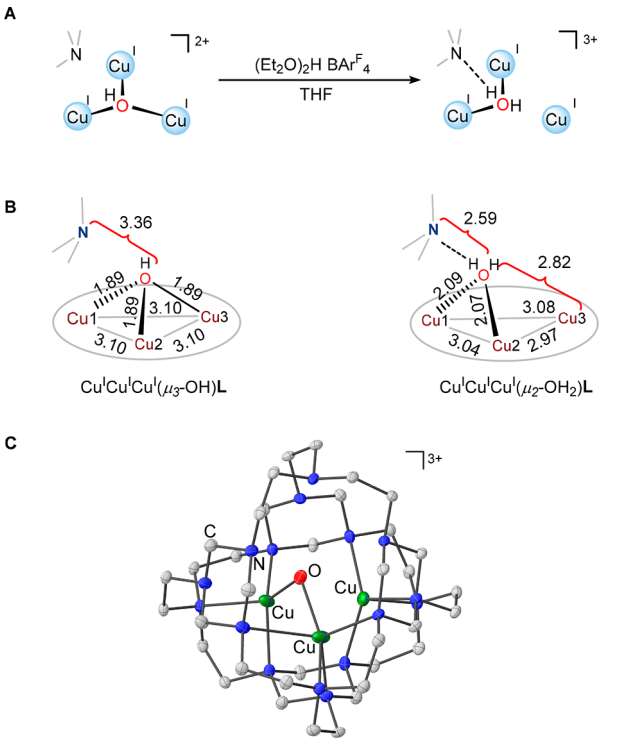

Figure 4. (A) Synthesis of $Cu^ICu^ICu^I(\mu_2\text{-}OH_2)\mathbf{L}$. (B) Bond distance (Å) information on $Cu^ICu^ICu^I(\mu_2\text{-}OH_2)\mathbf{L}$ and $Cu^ICu^ICu^I(\mu_2\text{-}OH_2)\mathbf{L}$. (C) Single-crystal XRD of $Cu^ICu^ICu^I(\mu_2\text{-}OH_2)\mathbf{L}$ with thermal ellipsoids of 50% probability. All H atoms, counteranions, and solvent molecules are omitted for clarity.

μ_3-OH (Figure 3C). The assignment of μ_3-O is further supported by the off-trend Cu−O and Cu···Cu distances at the II,II,II state (Figure 3D). The Cu···Cu and Cu−O distances generally increase with higher oxidation states due to the stronger Coulombic repulsion.[22] However, the II,II,II state does not follow this trend. Both Cu···Cu and Cu−O distances at the II,II,II state are shorter compared to the II,II,I state (Figure 3D), suggesting the charge of the central ligand increased from μ_3-OH^- to μ_3-O^{2-}, which results in a contraction of the tricopper cluster due to the stronger interactions between Cu^{II} and μ_3-O^{2-}. The intramolecular proton transfer (IPT) from μ_3-OH to the top of **L** is likely due to the increased acidity of the μ_3-OH at the II,II,II state. We were unable to measure the pK_a of the μ_3-OH^- motif because the acidic proton is buried inside the cryptand. Nonetheless, the pK_a of a similar $[Cu^{II}_3(\mu_3\text{-}OH)]^{5+}$ cluster has been reported by Suh et al. to be ca. 4.65 in H_2O,[23] which is much lower than that of TREN-H^+ (pK_a = ca. 10.27 in H_2O).[24] Conversely, backward IPT from **LH** to the μ_3-O is expected if the tricopper cluster is reduced from II,II,II to a lower oxidation state due to the increasing basicity of μ_3-O (*vide infra*).

$[TREN_4Cu^ICu^ICu^I(\mu_2\text{-}OH_2)]^{3+}$ as a Synthetic Model for FR. The fully reduced TNC features a tricopper I,I,I cluster with a H_2O ligand (Figure 1B). To prepare a synthetic model for **FR**, we treated the $[TREN_4Cu^ICu^ICu^I(\mu_3\text{-}OH)](BAr^F_4)_2$ complex ($Cu^ICu^ICu^I(\mu_3\text{-}OH)\mathbf{L}$, BAr^F_4 = 3,5-bis-(trifluoromethyl)phenyl)borate)[22] with one equivalent of Brookhart's acid $[(Et_2O)_2H]BAr^F_4$ in tetrahydrofuran (THF) (Figure 4A). The resulting colorless solid was crystallized from acetone after a counteranion exchange with PF_6^- (see the Supporting Information). ^{1}H NMR analysis of the product (Figure S3B, red spectrum) shows several sharp ^{1}H peaks, distinct from the broad resonances of $Cu^ICu^ICu^I(\mu_3\text{-}OH)\mathbf{L}$ (Figure S3B, blue spectrum), suggesting the protonated tricopper I,I,I complex is more rigid and has a lower symmetry than $Cu^ICu^ICu^I(\mu_3\text{-}OH)\mathbf{L}$. Importantly, the OH signal of μ_3-OH (1H, 1.35 ppm) has shifted downfield (2H, 9.15 ppm), indicating conversion of μ_3-OH to μ-OH_2. The assignment of the μ-OH_2 peak at 9.15 ppm was confirmed by a deuterium-labeling experiment (Figure S22). The significant downfield chemical shift suggests the μ-OH_2 motif is hydrogen-bonded to a nitrogen atom from the top TREN.

Single-crystal X-ray diffraction analysis of the colorless crystals grown from acetone shows a tricopper I,I,I complex with a μ_2-OH_2 ligand bridging between two Cu^I centers (Figure 4C). The remaining Cu^I does not interact with the O atom (Figure 4B, right, Cu3···O: 2.82 Å) and adopts a distorted tetrahedral geometry with four TREN nitrogen donors. Compared to the Cu···O distances in $Cu^ICu^ICu^I(\mu_3\text{-}OH)\mathbf{L}$ (Figure 4B, left, Cu···O: 1.89 Å) with one negative charged μ-OH ligand, the elongated Cu···O distances (Figure 4B, right, Cu1···O: 2.09 Å, Cu2···O: 2.07 Å) in $Cu^ICu^ICu^I(\mu_2\text{-}OH_2)\mathbf{L}$ suggest weaker interactions between copper atoms and the neutral μ-OH_2 ligand. Based on the three outer-sphere counterions and two protons of the aqua ligand, the product is formulated as $Cu^ICu^ICu^I(\mu_2\text{-}OH_2)\mathbf{L}$. One H atom on μ_2-OH_2 is hydrogen-bonded to a TREN nitrogen with a N−O distance

https://doi.org/10.1021/jacs.1c10948
J. Am. Chem. Soc. 2022, 144, 1709−1717

of 2.59 Å, which removes the C_3 symmetry typically observed in $TREN_4$ tricopper μ-OH and μ-O clusters (Figure 4C).[22] The low-symmetry X-ray diffraction (XRD) structure of $Cu^ICu^ICu^I(\mu_2\text{-}OH_2)$**L** is reflected by the well-resolved methylene (CH_2) ^{1}H NMR resonances (Figure S3). Nonetheless, the single ^{1}H NMR peak of μ-OH_2 indicates rapid exchange of the two protons residing on the μ_2-OH_2 ligand (Figure 4C).

Cyclic Voltammetry Study of Tricopper Cryptate. While many synthetic tricopper I,I,I complexes can model the conversion of **FR** to **NI**, i.e., the activation of O_2 at tricopper I,I,I to afford tricopper II,II,II μ-O or μ-OH species,[25−34] none can mimic the reductive regeneration of **FR** from **NI**, which is equally essential for catalytic oxygen reduction reaction (ORR). Most of the synthetic tricopper complexes are not redox-active, whereas the regeneration of **FR** consists of a formal three-electron and three-proton transfer that traverses four discrete oxidation states from II,II,II to I,I,I. The isolated environment of $TREN_4$ not only enables reversible redox behavior but also allows precise control of the total number of protons that can access the tricopper cluster. Proton(s) in $TREN_4$ can reside on either the μ_3-O/μ_3-OH or the top TREN as ammonium, giving four possible "protonation states", noted as [$Cu_3(\mu_3\text{-}O)$]**LH**, [$Cu_3(\mu_3\text{-}OH)$]**L** (Figure 5A), [$Cu_3(\mu_3\text{-}OH)$]**LH**, and [$Cu_3(\mu_2\text{-}OH_2)$]**L** (Figure 6A). Theoretically,

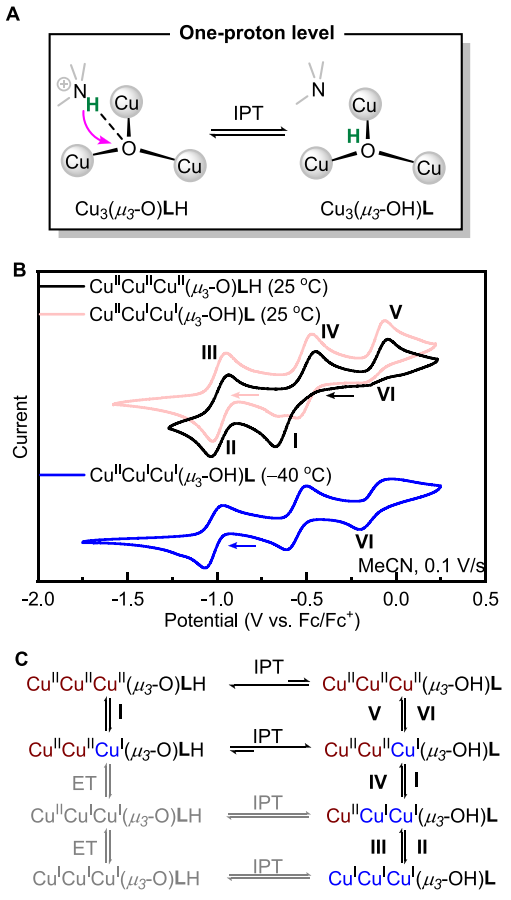

Figure 5. (A) Two possible protonation states of the tricopper cluster at the one-proton level. (B) CV of the tricopper complex at the one-proton level. Black: $Cu^{II}Cu^{II}Cu^{II}(\mu_3\text{-}O)$**LH** at 25 °C. Red: $Cu^{II}Cu^{II}Cu^{I}(\mu_3\text{-}OH)$**L** at 25 °C. Blue: $Cu^{II}Cu^{I}Cu^{I}(\mu_3\text{-}OH)$**L** at −40 °C. (C) Proposed redox mechanism of tricopper cryptate at the one-proton level. Species in gray are not observed.

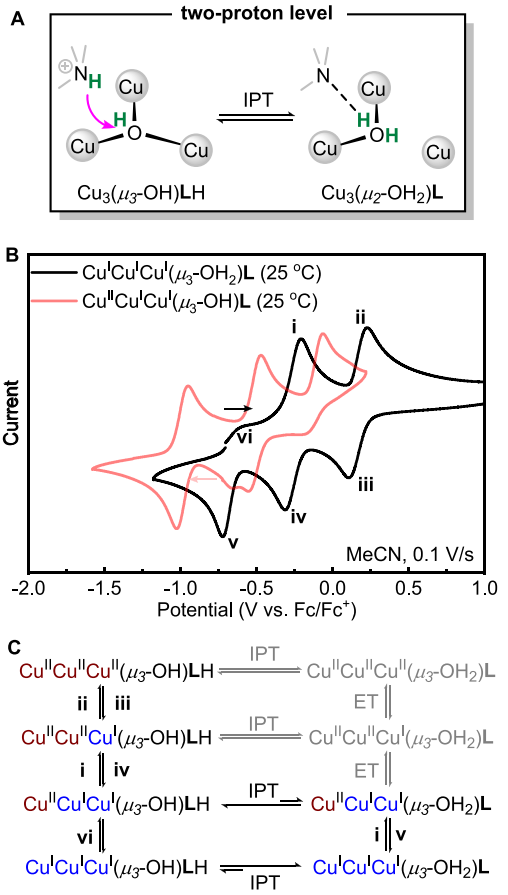

Figure 6. (A) Two possible protonation states of the tricopper cluster at the two-proton level. (B) Comparison of the CV of the tricopper complex at the two-proton level (black) and one-proton level (red). (C) Proposed redox mechanism of tricopper cryptate at the two-proton level. Species in gray are not observed.

the tricopper complex at each protonation state could access four oxidation states from II,II,II to I,I,I, giving rise to a total of 16 unique species (Figure 5C and Figure 6C). However, some combinations of protonation and oxidation states are too reactive to be observed (gray) and quickly converted to other species via intramolecular proton transfer or disproportionation reaction. To understand the conversion between these 16 possible species, we performed cyclic voltammetry (CV) studies of the tricopper complexes at one-proton and two-proton levels.

At the one-proton level, the CV of $Cu^{II}Cu^{II}Cu^{II}(\mu_3\text{-}O)$**LH** shows two reduction events at −0.66 V (I) and −1.0 V (II) vs Fc/Fc^+ (Figure 5B, black trace). Based on our previous work, the cathodic wave II at −1.0 V is from the reduction of $Cu^{II}Cu^ICu^I(\mu_3\text{-}OH)$**L** to $Cu^ICu^ICu^I(\mu_3\text{-}OH)$**L**. Therefore, the reduction I at −0.66 V should be assigned as the two-electron reduction of $Cu^{II}Cu^{II}Cu^{II}(\mu_3\text{-}O)$**LH** to $Cu^{II}Cu^ICu^I(\mu_3\text{-}OH)$**L**. Notably, this two-electron reduction process is coupled with an intramolecular proton transfer from **LH** to μ_3-O. During the reverse scan, the three one-electron oxidations were observed at −0.95 V (III), −0.47 V (IV), and −0.06 V (IV) vs Fc/Fc^+ (Figure 5B, black), which matches those observed from the cyclic voltammogram of $Cu^{II}Cu^ICu^I(\mu_3\text{-}OH)$**L** (Figure 5B, red).[22] Anodic waves III, IV, and V are assigned to the consecutive oxidation of $Cu^ICu^ICu^I(\mu_3\text{-}OH)$**L** to $Cu^{II}Cu^ICu^I(\mu_3\text{-}OH)$**L**, $Cu^{II}Cu^{II}Cu^I(\mu_3\text{-}OH)$**L**, and eventually

https://doi.org/10.1021/jacs.1c10948
J. Am. Chem. Soc. 2022, 144, 1709−1717

$Cu^{II}Cu^{II}Cu^{II}(\mu_3\text{-OH})$**L**, respectively. The last oxidation from $Cu^{II}Cu^{II}Cu^{I}(\mu_3\text{-OH})$**L** to $Cu^{II}Cu^{II}Cu^{II}(\mu_3\text{-OH})$**L** (Figure 5B, V) is irreversible, suggesting the electron transfer is coupled with an IPT to afford $Cu^{II}Cu^{II}Cu^{II}(\mu_3\text{-O})$**LH** (Figure 5C). This hypothesis was confirmed by a CV experiment at low temperature (Figure 5B, blue). At −40 °C, the IPT process slows down, and the cathodic wave for the reduction of $Cu^{II}Cu^{II}Cu^{II}(\mu_3\text{-OH})$**L** was revealed at −0.19 V (Figure 5B, blue, VI).

At the two-proton level, the CV of $Cu^{I}Cu^{I}Cu^{I}(\mu_2\text{-OH}_2)$ shows two oxidation peaks at −0.20 V (i) and 0.24 V (ii) vs Fc/Fc^{+} (Figure 6B, black). During the reverse scan, three one-electron reductions at 0.10 V (iii), −0.32 V (iv), and −0.72 V (v) vs Fc/Fc^{+} were observed (Figure 6B, black). Overall, the CV of the tricopper complex at the two-proton level (Figure 6B, black) shifted anodically by ca. 200 mV compared to that at the one-proton level (Figure 6B red), reflecting the increased charge as a result of protonation.[35] The anodic wave i at −0.20 V can be assigned to a two-electron oxidation coupled with IPT from $Cu^{I}Cu^{I}Cu^{I}(\mu_2\text{-OH}_2)$**L** to $Cu^{II}Cu^{II}Cu^{I}(\mu_3\text{-OH})$**LH**. The following oxidation ii is from $Cu^{II}Cu^{II}Cu^{I}(\mu_3\text{-OH})$**LH** to $Cu^{II}Cu^{II}Cu^{II}(\mu_3\text{-OH})$**LH**. The three sequential cathodic waves iii, iv, and v in the reverse scan are assigned to the sequential reduction from $Cu^{II}Cu^{II}Cu^{II}(\mu_3\text{-OH})$**LH** to $Cu^{I}Cu^{I}Cu^{I}(\mu_2\text{-OH}_2)$**L**, where the last reduction v is believed to couple with an IPT from **L**H to μ_3-OH. The small anodic wave at −0.61 V (vi) is assigned to the oxidation of $Cu^{I}Cu^{I}Cu^{I}(\mu_3\text{-OH})$**LH** (see the Supporting Information, Figure S27).

In summary, the CV study shows that the proton affinity of the μ_3-O/μ_3-OH ligand in the tricopper complex changes as a function of the oxidation states. On two occasions, the electron transfers are coupled with intramolecular proton transfer, i.e., $Cu^{II}Cu^{II}Cu^{II}(\mu_3\text{-O})$**LH** to $Cu^{II}Cu^{II}Cu^{I}(\mu_3\text{-OH})$**L** at the one-proton level and $Cu^{II}Cu^{I}Cu^{I}(\mu_3\text{-OH})$**LH** to $Cu^{I}Cu^{I}Cu^{I}(\mu_2\text{-OH}_2)$**L** at the two-proton level. The mechanisms of these two PCET reactions were further investigated with spectroscopy.

PCET from $Cu^{II}Cu^{II}Cu^{II}(\mu_3\text{-O})$LH to $Cu^{II}Cu^{II}Cu^{I}(\mu_3\text{-OH})$L. To understand the mechanism of PCET from $Cu^{II}Cu^{II}Cu^{II}(\mu_3\text{-O})$**LH** to $Cu^{II}Cu^{II}Cu^{I}(\mu_3\text{-OH})$**L**, we examined the chemical reduction of $Cu^{II}Cu^{II}Cu^{II}(\mu_3\text{-O})$**LH** at low temperature, attempting to capture the intermediate $Cu^{II}Cu^{II}Cu^{I}(\mu_3\text{-O})$**LH** before IPT. Treatment of $Cu^{II}Cu^{II}Cu^{II}(\mu_3\text{-O})$**LH** with one equivalent of cobaltocene (Cp_2Co) at −90 °C affords a stable species with a UV−vis band at 630 nm (ε = 3150 M^{-1} cm^{-1}), which was assigned at $Cu^{II}Cu^{II}Cu^{I}(\mu_3\text{-O})$**LH**. Warming up the solution to −80 °C leads to the consumption of $Cu^{II}Cu^{II}Cu^{I}(\mu_3\text{-O})$**LH** due to IPT. However, the expected $Cu^{II}Cu^{II}Cu^{I}(\mu_3\text{-OH})$**L** was not observed. Instead, the final UV−vis spectrum (Figure 7A, green traces) can be deconvoluted into a mixture (red dashed) of $Cu^{II}Cu^{II}Cu^{II}(\mu_3\text{-O})$**LH** (blue) and $Cu^{II}Cu^{I}Cu^{I}(\mu_3\text{-OH})$**L** (orange) in a 1:1 ratio. The overall reaction can be rationalized by a disproportionation mechanism (Figure 7B): (i) $Cu^{II}Cu^{II}Cu^{II}(\mu_3\text{-O})$**LH** is reduced by Cp_2Co to $Cu^{II}Cu^{II}Cu^{I}(\mu_3\text{-O})$**LH**, which undergoes (ii) IPT to afford $Cu^{II}Cu^{II}Cu^{I}(\mu_3\text{-OH})$**L**, which is (iii) immediately reduced by another equivalent of $Cu^{II}Cu^{II}Cu^{I}(\mu_3\text{-O})$**LH** to $Cu^{II}Cu^{I}Cu^{I}(\mu_3\text{-OH})$**L**. The disproportionation reaction also regenerates a half-equivalent of $Cu^{II}Cu^{II}Cu^{II}(\mu_3\text{-O})$**LH**, finally resulting in a 1:1 mixture of $Cu^{II}Cu^{I}Cu^{I}(\mu_3\text{-OH})$**L** and $Cu^{II}Cu^{II}Cu^{II}(\mu_3\text{-O})$**LH**. This proposed mechanism is consistent with the redox potentials of $Cu^{II}Cu^{II}Cu^{I}(\mu_3\text{-OH})$**L**/$Cu^{II}Cu^{I}Cu^{I}(\mu_3\text{-OH})$**L** (−0.52 V) and $Cu^{II}Cu^{II}Cu^{II}(\mu_3\text{-O})$**LH**/$Cu^{II}Cu^{II}Cu^{I}(\mu_3\text{-O})$**LH** (−0.66 V, Figure S26), suggesting the proposed electron transfer (Figure 7B, step III) is thermodynamically favorable.

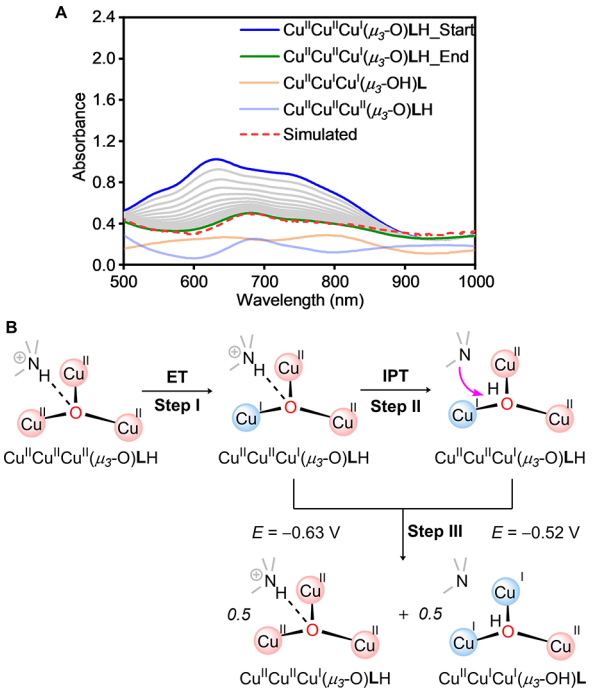

Figure 7. (A) UV−vis spectrum of treatment of $Cu^{II}Cu^{II}Cu^{I}(\mu_3\text{-O})$**LH** with one equivalent of Cp_2Co at −80 °C. The final spectrum after the disproportionation (green trace) can be fitted with a 1:1 ratio of $Cu^{II}Cu^{I}Cu^{I}(\mu_3\text{-OH})$**L** and $Cu^{II}Cu^{II}Cu^{II}(\mu_3\text{-O})$**LH** (red dashed trace). (B) Proposed mechanism of the one-electron reduction of $Cu^{II}Cu^{II}Cu^{II}(\mu_3\text{-O})$**LH** to $Cu^{II}Cu^{I}Cu^{I}(\mu_3\text{-OH})$**L** and $Cu^{II}Cu^{II}Cu^{II}(\mu_3\text{-O})$ **LH** in a 1:1 ratio.

The PCET from $Cu^{II}Cu^{II}Cu^{II}(\mu_3\text{-O})$**LH** to $Cu^{II}Cu^{II}Cu^{I}(\mu_3\text{-OH})$**L** can occur in concerted or stepwise mechanisms, i.e., initial transfer of a proton followed by electron transfer (PT−ET), electron transfer followed by proton transfer (ET−PT), or concerted proton−electron transfer (CPET), where a proton and an electron are transferred in a single kinetic step (Figure 8A).[13,19,21] Both CV and UV−vis studies at low temperature suggest an ET−PT mechanism since the reduction of $Cu^{II}Cu^{II}Cu^{II}(\mu_3\text{-O})$**LH** initially affords the intermediate $Cu^{II}Cu^{II}Cu^{I}(\mu_3\text{-O})$**LH**, which readily converts to $Cu^{II}Cu^{II}Cu^{I}(\mu_3\text{-OH})$**L**. The kinetics of the IPT from $Cu^{II}Cu^{II}Cu^{I}(\mu_3\text{-O})$**LH** to $Cu^{II}Cu^{II}Cu^{I}(\mu_3\text{-OH})$**L** was investigated by variable-temperature UV−vis spectroscopy by monitoring the decay of $Cu^{II}Cu^{II}Cu^{I}(\mu_3\text{-O})$**LH**. The first-order rate constant of IPT was determined from −50 to −80 °C (see the Supporting Information). According to the Eyring analysis (Figure 8B), the activation enthalpy ($\Delta H^{\ddagger}$) and entropy ($\Delta S^{\ddagger}$) for IPT at the II,II,I state are 9.9 ± 0.8 kcal/mol and −20 ± 4 cal/(mol K), respectively.

PCET from $Cu^{II}Cu^{I}Cu^{I}(\mu_3\text{-OH})$LH to $Cu^{I}Cu^{I}Cu^{I}(\mu_2\text{-OH}_2)$L. Analogously, the reduction of $Cu^{II}Cu^{I}Cu^{I}(\mu_3\text{-OH})$**LH** to $Cu^{I}Cu^{I}Cu^{I}(\mu_2\text{-OH}_2)$**L** can proceed through an ET−PT, PT−ET, or CPET mechanism. Treatment of $Cu^{II}Cu^{I}Cu^{I}(\mu_3\text{-OH})$**L** with one equivalent of $[(Et_2O)_2H]BAr^{F}_4$ at 20 °C did not result in detectable spectral changes, suggesting the protonation likely occurred at the top TREN to give $Cu^{II}Cu^{I}Cu^{I}(\mu_3\text{-OH})$**LH** (Figure 9A). ^{1}H NMR analysis of the reaction mixture shows the same paramagnetic resonances similar to

https://doi.org/10.1021/jacs.1c10948
J. Am. Chem. Soc. 2022, 144, 1709−1717

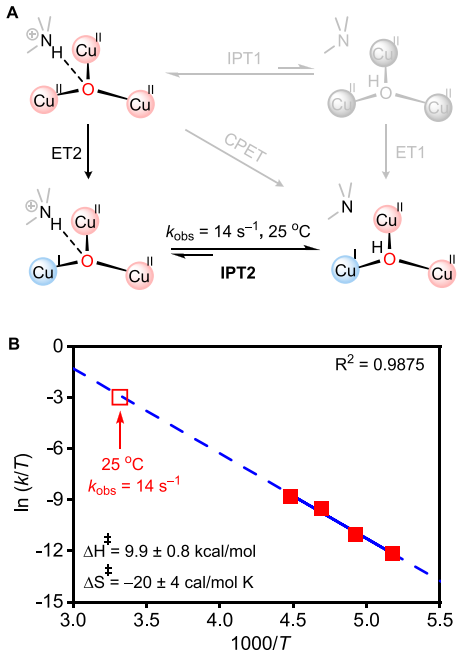

Figure 8. (A) Mechanisms of PCET from $Cu^{II}Cu^{II}Cu^{II}(\mu_3\text{-O})$**LH** to $Cu^{II}Cu^{II}Cu^{I}(\mu_3\text{-OH})$**L**. (B) Eyring plot of IPT2 from $Cu^{II}Cu^{II}Cu^{II}(\mu_3\text{-O})$**LH** to $Cu^{II}Cu^{II}Cu^{I}(\mu_3\text{-OH})$**L** (red).

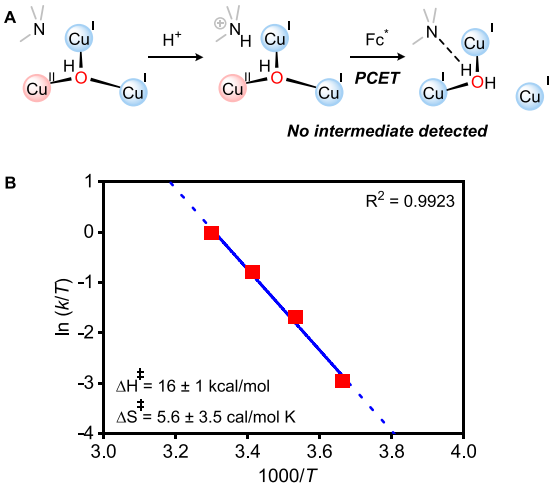

Figure 9. (A) Protonation of $Cu^{II}Cu^{I}Cu^{I}(\mu_3\text{-OH})$**L** and subsequent PCET conversion to $Cu^{II}Cu^{I}Cu^{I}(\mu_3\text{-OH}_2)$**L**. (B) Eyring plot of PCET from $Cu^{II}Cu^{I}Cu^{I}(\mu_3\text{-OH})$**LH** to $Cu^{I}Cu^{I}Cu^{I}(\mu_2\text{-OH}_2)$**L** with decamethylferrocene (Fc*) as the reductant.

those of tricopper II,I,I starting materials (Figure S18), further supporting that the proton was transferred to the top TREN instead of the $Cu^{II}Cu^{I}Cu^{I}(\mu_3\text{-OH})$ core. Addition of decamethylferrocene (Fc*) to $Cu^{II}Cu^{I}Cu^{I}(\mu_3\text{-OH})$**LH** led to its PCET conversion to $Cu^{I}Cu^{I}Cu^{I}(\mu_2\text{-OH}_2)$**L** in quantitative yield, as evidenced by ^{1}H NMR analysis (Figure S18, spectrum 3). However, no intermediate, e.g., $Cu^{I}Cu^{I}Cu^{I}(\mu_2\text{-OH})$**LH** or $Cu^{II}Cu^{I}Cu^{I}(\mu_2\text{-OH}_2)$**L**, was detected by UV–vis, ^{1}H NMR, and bulk electrolysis study (Figure S25). Nonetheless, the rate of PCET can be determined with variable-temperature UV–vis by recording the spectral decay of $Cu^{II}Cu^{I}Cu^{I}(\mu_3\text{-OH})$**LH** (Figure S13) from 0 to 30 °C. Eyring analysis reveals $\Delta H^{\ddagger}$ = 16 ± 1 kcal/mol and $\Delta S^{\ddagger}$ = 5.6 ± 3.5 cal/(mol K) for the PCET (Figure 9B).

Since no reaction intermediate was detected, further kinetic analysis and CV simulation were performed to investigate the mechanism of the PCET from $Cu^{II}Cu^{I}Cu^{I}(\mu_3\text{-OH})$**LH** to $Cu^{I}Cu^{I}Cu^{I}(\mu_2\text{-OH}_2)$**L**. To investigate a stepwise ET–PT mechanism, we attempted to generate the putative intermediate $Cu^{I}Cu^{I}Cu^{I}(\mu_2\text{-OH})$**LH** from protonation of $Cu^{I}Cu^{I}Cu^{I}(\mu_2\text{-OH})$**L** (Figure 10). The reaction of

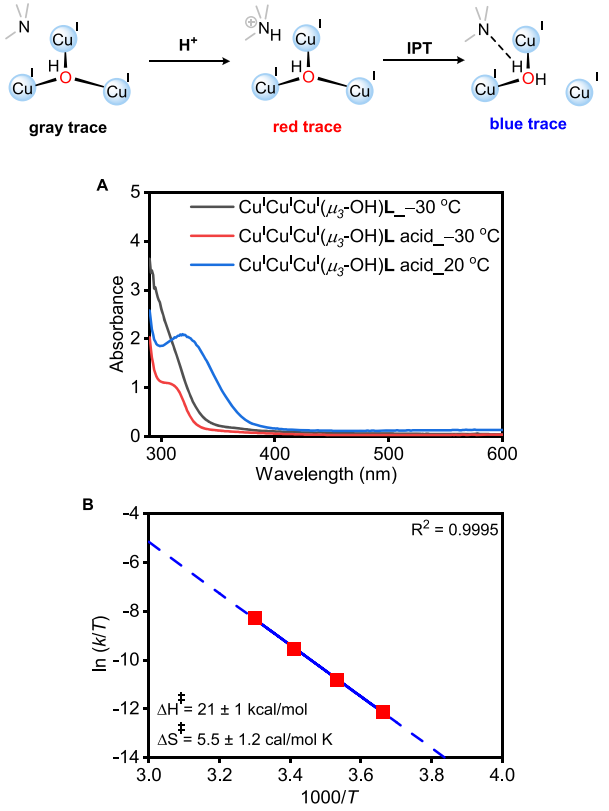

Figure 10. (A) UV–vis spectrum of the reaction between $Cu^{I}Cu^{I}Cu^{I}(\mu_3\text{-OH})$**LH** and $[(Et_2O)_2H]BAr^F{}_4$ at −30 °C (blue) and 20 °C (red). (B) Eyring plot of IPT steps from $Cu^{I}Cu^{I}Cu^{I}(\mu_3\text{-OH})$**LH** to $Cu^{I}Cu^{I}Cu^{I}(\mu_2\text{-OH}_2)$**L**.

$Cu^{I}Cu^{I}Cu^{I}(\mu_3\text{-OH})$**L** and $[(Et_2O)_2H]$ $BAr^F{}_4$ at −30 °C affords a new species with absorbance at 310 nm (ε = 1428 M^{-1} cm^{-1}, red trace), which converts to $Cu^{I}Cu^{I}Cu^{I}(\mu_2\text{-OH}_2)$**L** ($\lambda$ = 320 nm, ε = 1850 M^{-1} cm^{-1}, blue trace) at 20 °C (Figure 10A). The ^{1}H NMR spectrum of the intermediate at −50 °C shows two new broad peaks at 9.59 and 9.42 ppm in a 1:1 ratio (Figure S20), consistent with a $Cu^{I}Cu^{I}Cu^{I}(\mu_3\text{-OH})$**LH** species with an ammonium R_3N^+H motif hydrogen-bonded to μ_2-OH (Figure 10). The kinetics of IPT from $Cu^{I}Cu^{I}Cu^{I}(\mu_3\text{-OH})$**LH** to $Cu^{I}Cu^{I}Cu^{I}(\mu_2\text{-OH}_2)$**L** was studied by monitoring the UV–vis spectrum of the reaction at different temperatures (Figure 10B). The first-order rate constant of IPT from $Cu^{I}Cu^{I}Cu^{I}(\mu_3\text{-OH})$**LH** to $Cu^{I}Cu^{I}Cu^{I}(\mu_2\text{-OH}_2)$**L** is 0.039 s^{-1} at 25 °C (calculated from Eyring analysis, Figure 10B), which is slower than the rate of PCET (0.34 s^{-1}, 25 °C) (calculated based on a Fc* concentration of 1.62 mM) at the same temperature, strongly suggesting the $Cu^{I}Cu^{I}Cu^{I}(\mu_3\text{-OH})$**LH** is not an intermediate during the PCET from $Cu^{II}Cu^{I}Cu^{I}(\mu_3\text{-OH})$**LH** to $Cu^{I}Cu^{I}Cu^{I}(\mu_2\text{-OH}_2)$**L**. The stepwise ET–PT mechanism is unlikely due to the slow rate of IPT (Figure 11A).

With a PCET rate of 207 M^{-1} s^{-1} at 25 °C from $Cu^{II}Cu^{I}Cu^{I}(\mu_3\text{-OH})$**LH** to $Cu^{I}Cu^{I}Cu^{I}(\mu_2\text{-OH}_2)$**L** (Figure 9A)

https://doi.org/10.1021/jacs.1c10948
J. Am. Chem. Soc. 2022, 144, 1709–1717

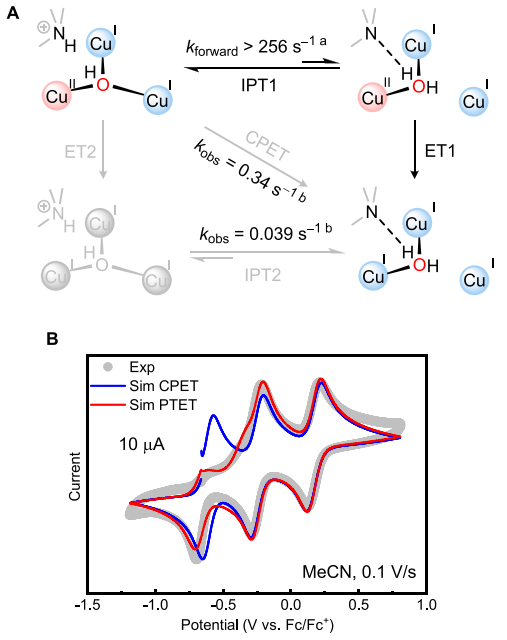

Figure 11. (A) Mechanisms of PCET from $Cu^{II}Cu^{I}Cu^{I}(\mu_3\text{-OH})$**LH** to $Cu^{I}Cu^{I}Cu^{I}(\mu_2\text{-OH}_2)$**L**. (B) CV simulation results with a PT−ET mechanism (red) or a CPET mechanism (blue). The experimental cyclic voltammogram is shown in thick gray. [a]Rate constant determined by CV simulation (25 °C). [b]Rate constant determined by UV−vis kinetic experiment and converted to 25 °C by an Eyring plot.

and an estimated K_{eq} of ca. 10^{-6} for the IPT between $Cu^{II}Cu^{I}Cu^{I}(\mu_3\text{-OH})$**LH** and $Cu^{II}Cu^{I}Cu^{I}(\mu_3\text{-OH}_2)$**L** (Table S5), neither the CPET nor PT−ET mechanism can be excluded based on a thermodynamic exclusionary argument (see the Supporting Information, Scheme S1). Therefore, we turn to CV simulation of $Cu^{I}Cu^{I}Cu^{I}(\mu_3\text{-OH}_2)$**L** at room temperature to differentiate the two possible mechanisms (see the Supporting Information).[36,37] The simulated CV profile with a CPET mechanism reveals the general redox behavior of $Cu^{I}Cu^{I}Cu^{I}(\mu_3\text{-OH}_2)$**L**. However, the detailed voltammetric features are not fully coincident with the experimental results (Figure 11B, blue). For example, the simulated voltammogram cannot reproduce the irreversible reduction around −0.7 V. In contrast, CV simulations with a PT−ET mechanism successfully replicated the experimental data as shown in Figure 11B (red). The FitSpace analysis of the CV simulation indicates the minimum forward rate constant for IPT1 is 256 s^{-1}, which is still much faster than IPT2 (0.039 s^{-1}, 25 °C), explaining why the PT−ET pathway is favored over ET−PT (Figure 11A). The simulated K_{eq} of IPT1 and IPT2 are 6.5 × 10^{-6} and 8.8, respectively, suggesting the reduction of the tricopper cluster changes the pK_a of the μ_2-OH_2 ligand by seven units.

DISCUSSION

The reduction of **NI** back to **FR** in MCOs involves rapid transfer of three protons and three electrons. All three ETs are coupled with PT (Figure 1B).[8,9] Our tricopper model system demonstrates a similar process involving three electrons and two protons from $Cu^{II}Cu^{II}Cu^{II}(\mu\text{-O})$ to $Cu^{I}Cu^{I}Cu^{I}(\mu\text{-OH}_2)$ (Figure 12). We successfully reproduce the first and last PCET in MCOs, where both processes involve PT to the central μ_3-O ligand. Solomon et al. proposed that the high basicity of the μ_3-O motif in **NI** plays a critical role in facilitating rapid intramolecular electron transfer from the T1 site to the TNC site.[8,9,38] The reduction of the resting oxidized state, which lacks the μ_3-O ligand, is 10^3 times slower. Our findings support the critical role of the tricopper μ_3-O motif: the reduction of the tricopper center causes a substantial increase in the basicity of the central ligand μ_3-O or μ_3-OH ligand, which provides the driving force for spontaneous IPT from the secondary coordination sphere.

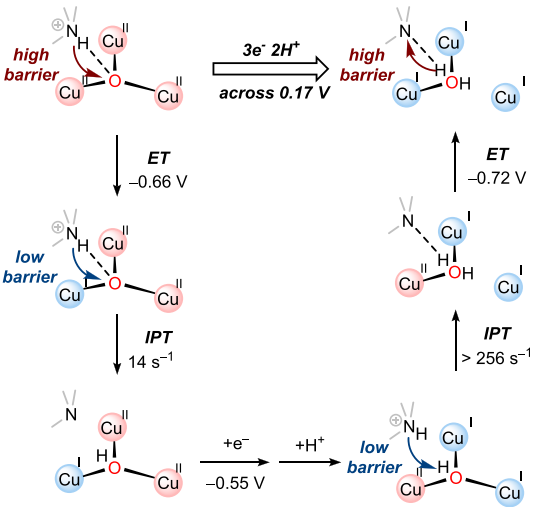

Figure 12. Summary of three-electron and two-proton conversion from a $Cu^{II}Cu^{II}Cu^{II}(\mu_3\text{-O})$**LH** to a $Cu^{I}Cu^{I}Cu^{I}(\mu_2\text{-OH}_2)$**L** within 0.17 V.

The mechanisms of the three-electron and two-proton conversion from a $Cu^{II}Cu^{II}Cu^{II}(\mu_3\text{-O})$**L** to a $Cu^{I}Cu^{I}Cu^{I}(\mu_2\text{-OH}_2)$**L** have been established via spectroscopic characterization of seven intermediates. An ET−PT mechanism was observed from $Cu^{II}Cu^{II}Cu^{II}(\mu_3\text{-O})$**LH** to $Cu^{II}Cu^{II}Cu^{I}(\mu_3\text{-OH})$**L** state, while a PT−ET mechanism was established from $Cu^{II}Cu^{I}Cu^{I}(\mu_3\text{-OH})$**LH** to $Cu^{I}Cu^{I}Cu^{I}(\mu_3\text{-OH}_2)$**L** (Figure 12). Mechanism switch-overs between CPET, PT−ET, and ET−PT within the same system[37] have been observed as a function of temperature,[39] Lewis acid addition,[40] ligand basicity,[41] and substrate acidity.[42] We reason that the mechanistic dichotomy in our system is due to various IPT rates at different oxidation states. The rate constant of IPT from μ_3-OH to μ_2-OH_2 at II,I,I (>256 s^{-1}, 25 °C) is ca. 6000 times faster than that at I,I,I (0.039 s^{-1}, 25 °C), likely due to the easier Cu−O dissociation as a result of the weaker Cu−O bond at the II,I,I state. Therefore, the PT−ET mechanism provides kinetic advantages by bypassing a high IPT barrier at the I,I,I state. Analogously, the ET−PT mechanism from μ_3-O to μ_2-OH bypasses IPT at the II,II,II state, which also features a strong Cu−O bond. In summary, IPTs are faster at the II,I,I and II,II,I state due to the ease of structural rearrangement as the result of the weaker Cu−O bonds (Figure 3D).

To the best of our knowledge, the redox potentials of various tricopper oxo/hydroxo intermediates in MCOs have not been reported. Nonetheless, they are expected to be more anodic than that of the T1 site (300−800 mV vs SHE),[43,44] since intramolecular electron transfers T1 to the TNC site are thermodynamically favorable. The redox potential of our tricopper μ-OH complexes in aqueous phosphate buffer is from −550 to 330 mV (vs SHE),[22] suggesting they are harder to reduce than tricopper oxo/hydroxo intermediates in MCOs,

https://doi.org/10.1021/jacs.1c10948
J. Am. Chem. Soc. 2022, 144, 1709−1717

perhaps due to the electron-donating nature of amine ligands in $TREN_4$. Despite these potential deviations, the redox behavior of our tricopper complex at different protonated states reflects the redox potential leveling effect of intramolecular proton transfer. At the same proton level, such as $Cu_3(\mu_3\text{-OH})$, the potential difference between II,II,II and I,I,I is around 0.9 V. However, when proton transfer is involved, the complete reduction of II,II,II to I,I,I state can be accomplished in a narrow 170 mV range (Figure 12). The observation of a redox-leveling effect in synthetic tricopper clusters should enable new strategies to control proton-coupled multiple electron transfer to metal clusters.

CONCLUSION

In conclusion, our synthetic tricopper complexes successfully replicated MCOs' ability to accumulate multiple redox equivalents within a narrow potential range. The three-electron two-proton PCET conversion of $Cu^{II}Cu^{II}Cu^{II}(\mu_3\text{-O})\mathbf{L}$ to $Cu^{I}Cu^{I}Cu^{I}(\mu_2\text{-OH}_2)\mathbf{L}$ reflects the "redox potential leveling" effect, which is crucial for biological metal clusters to accumulate multiple redox equivalents. The difference in reduction potentials from II,II,II and I,I,I is reduced from 0.9 to 0.17 V in the presence of a simple proton relay. Our study shows the interdependent nature of ET and PT during the conversions between multimetallic oxo M_x–O, hydroxo M_x–OH, and aqua M_x–OH_2 complexes, which are central to oxygen reduction reaction and oxygen evolution reaction, two of the most important bioenergetic processes.

ASSOCIATED CONTENT

Supporting Information

The Supporting Information is available free of charge at https://pubs.acs.org/doi/10.1021/jacs.1c10948.

Experimental details and characterization data, including X-ray crystallographic data for $Cu^{II}Cu^{II}Cu^{II}(\mu_3\text{-O})\mathbf{LH}$ and $Cu^{I}Cu^{I}Cu^{I}(\mu_2\text{-OH}_2)\mathbf{L}$ (PDF)

Accession Codes

CCDC 2111320 and 2111322 contain the supplementary crystallographic data for this paper. These data can be obtained free of charge via www.ccdc.cam.ac.uk/data_request/cif, or by emailing data_request@ccdc.cam.ac.uk, or by contacting The Cambridge Crystallographic Data Centre, 12 Union Road, Cambridge CB2 1EZ, UK; fax: +44 1223 336033.

AUTHOR INFORMATION

Corresponding Author

Shiyu Zhang − *Department of Chemistry and Biochemistry, The Ohio State University, Columbus, Ohio 43210, United States;* orcid.org/0000-0002-2536-4324; Email: zhang.8941@osu.edu

Authors

Weiyao Zhang − *Department of Chemistry and Biochemistry, The Ohio State University, Columbus, Ohio 43210, United States*

Curtis E. Moore − *Department of Chemistry and Biochemistry, The Ohio State University, Columbus, Ohio 43210, United States;* orcid.org/0000-0002-3311-7155

Complete contact information is available at: https://pubs.acs.org/10.1021/jacs.1c10948

Notes

The authors declare no competing financial interest.

ACKNOWLEDGMENTS

This material is based on work supported by the U.S. National Science Foundation under award no. CHE-1904560. The authors thank the Ohio State University Department Chemistry and Biochemistry for additional financial support.

REFERENCES

(1) Solomon, E. I.; Sundaram, U. M.; Machonkin, T. E. Multicopper Oxidases and Oxygenases. *Chem. Rev.* **1996**, *96*, 2563−2606.

(2) Ferreira, K. N.; Iverson, T. M.; Maghlaoui, K.; Barber, J. Architecture of the Photosynthetic Oxygen-Evolving Center. *Science.* **2004**, *303*, 1831−1838.

(3) Dobbek, H. Crystal Structure of a Carbon Monoxide Dehydrogenase Reveals a [Ni-4Fe-5S] Cluster. *Science* **2001**, *293*, 1281−1285.

(4) Burgess, B. K.; Lowe, D. J. Mechanism of Molybdenum Nitrogenase. *Chem. Rev.* **1996**, *96*, 2983−3011.

(5) Quintanar, L.; Stoj, C.; Wang, T. P.; Kosman, D. J.; Solomon, E. I. Role of Aspartate 94 in the Decay of the Peroxide Intermediate in the Multicopper Oxidase Fet3p. *Biochemistry* **2005**, *44*, 6081−6091.

(6) Augustine, A. J.; Quintanar, L.; Stoj, C. S.; Kosman, D. J.; Solomon, E. I. Spectroscopic and Kinetic Studies of Perturbed Trinuclear Copper Clusters: The Role of Protons in Reductive Cleavage of the O-O Bond in the Multicopper Oxidase Fet3p. *J. Am. Chem. Soc.* **2007**, *129*, 13118−13126.

(7) Augustine, A. J.; Kjaergaard, C.; Qayyum, M.; Ziegler, L.; Kosman, D. J.; Hodgson, K. O.; Hedman, B.; Solomon, E. I. Systematic Perturbation of the Trinuclear Copper Cluster in the Multicopper Oxidases: The Role of Active Site Asymmetry in Its Reduction of O_2 to H_2O. *J. Am. Chem. Soc.* **2010**, *132*, 6057−6067.

(8) Heppner, D. E.; Kjaergaard, C. H.; Solomon, E. I. Molecular Origin of Rapid versus Slow Intramolecular Electron Transfer in the Catalytic Cycle of the Multicopper Oxidases. *J. Am. Chem. Soc.* **2013**, *135*, 12212−12215.

(9) Heppner, D. E.; Kjaergaard, C. H.; Solomon, E. I. Mechanism of the Reduction of the Native Intermediate in the Multicopper Oxidases: Insights into Rapid Intramolecular Electron Transfer in Turnover. *J. Am. Chem. Soc.* **2014**, *136*, 17788−17801.

(10) Solomon, E. I.; Heppner, D. E.; Johnston, E. M.; Ginsbach, J. W.; Cirera, J.; Qayyum, M.; Kieber-Emmons, M. T.; Kjaergaard, C. H.; Hadt, R. G.; Tian, L. Copper Active Sites in Biology. *Chem. Rev.* **2014**, *114*, 3659−3853.

(11) Elwell, C. E.; Gagnon, N. L.; Neisen, B. D.; Dhar, D.; Spaeth, A. D.; Yee, G. M.; Tolman, W. B. Copper-Oxygen Complexes Revisited: Structures, Spectroscopy, and Reactivity. *Chem. Rev.* **2017**, *117*, 2059−2107.

(12) Reinhammar, B. R. M. Oxidation-Reduction Potentials of the Electron Acceptors in Laccases and Stellacyanin. *BBA - Bioenerg.* **1972**, *275*, 245−259.

(13) Weinberg, D. R.; Gagliardi, C. J.; Hull, J. F.; Murphy, C. F.; Kent, C. A.; Westlake, B. C.; Paul, A.; Ess, D. H.; Granville, D.; Meyer, T. J. Proton-Coupled Electron Transfer. *Chem. Rev.* **2012**, *112*, 4016−4093.

(14) Zhao, Q.; Betley, T. A. Synthesis and Redox Properties of Triiron Complexes Featuring Strong Fe−Fe Interactions. *Angew. Chemie Int. Ed.* **2011**, *50*, 709−712.

(15) De Ruiter, G.; Thompson, N. B.; Lionetti, D.; Agapie, T. Nitric Oxide Activation by Distal Redox Modulation in Tetranuclear Iron Nitrosyl Complexes. *J. Am. Chem. Soc.* **2015**, *137*, 14094−14106.

(16) Johnson, B. J.; Antholine, W. E.; Lindeman, S. V.; Mankad, N. P. A Cu_4S Model for the Nitrous Oxide Reductase Active Sites Supported Only by Nitrogen Ligands. *Chem. Commun.* **2015**, *51*, 11860−11863.

(17) Hernández Sánchez, R.; Zheng, S. L.; Betley, T. A. Ligand Field Strength Mediates Electron Delocalization in Octahedral

$[(HL)_2Fe_6(L\bullet)_m]^{N+}$ Clusters. *J. Am. Chem. Soc.* **2015**, *137*, 11126−11143.
(18) Arnett, C. H.; Chalkley, M. J.; Agapie, T. A Thermodynamic Model for Redox-Dependent Binding of Carbon Monoxide at Site-Differentiated, High Spin Iron Clusters. *J. Am. Chem. Soc.* **2018**, *140*, 5569−5578.
(19) Huynh, M. H. V; Meyer, T. J. Proton-Coupled Electron Transfer. *Chem. Rev.* **2007**, *107*, 5004−5064.
(20) Miyazaki, S.; Kojima, T.; Mayer, J. M.; Fukuzumi, S. Proton-Coupled Electron Transfer of Ruthenium(III)-Pterin Complexes: A Mechanistic Insight. *J. Am. Chem. Soc.* **2009**, *131*, 11615−11624.
(21) Warren, J. J.; Tronic, T. A.; Mayer, J. M.; Bond, S. V. G. Thermochemistry of Proton-Coupled Electron Transfer Reagents and Its Implications. *Chem. Rev.* **2010**, *110*, 6961−7001.
(22) Zhang, W.; Moore, C. E.; Zhang, S. Encapsulation of Tricopper Cluster in a Synthetic Cryptand Enables Facile Redox Processes from $Cu^ICu^ICu^I$ to $Cu^{II}Cu^{II}Cu^{II}$ states. *Chem. Sci.* **2021**, *12*, 2986−2992.
(23) Suh, M. P.; Han, M. Y.; Lee, J. H.; Min, K. S.; Hyeon, C. One-Pot Template Synthesis and Properties of a Molecular Bowl: Dodecaaza Macrotetracycle with μ^3-Oxo and μ^3-Hydroxo Tricopper-(II) Cores. *J. Am. Chem. Soc.* **1998**, *120*, 3819−3820.
(24) Nguyen, W. H. C. H.; Henni, A. Dissociation Constant (p Ka) and Thermodynamic Properties of 1,4-Bis(3-Aminopropyl) Piperazine, 1,3-Bis(Aminomethyl) Cyclohexane, Tris(2-Aminoethyl) Amine, and 1-Amino-4-Methyl Piperazine: Study of the Protonation Mechanism Using the Density Function Theo. *J. Chem. Eng. Data* **2020**, *65*, 2280−2290.
(25) Gupta, A. K.; Tolman, W. B. $Cu(I)/O_2$ Chemistry Using a β-Diketiminate Supporting Ligand Derived from N, N-Dimethylhydrazine: A $[Cu_3O_2]^{3+}$ Complex with Novel Reactivity. *Inorg. Chem.* **2012**, *51*, 1881−1888.
(26) Cole, A. P.; Root, D. E.; Mukherjee, P.; Solomon, E. I.; Stack, T. D. P. A Trinuclear Intermediate in the Copper-Mediated Reduction of O_2: Four Electrons from Three Coppers. *Science.* **1996**, *273*, 1848−1850.
(27) Thiyagarajan, N.; Janmanchi, D.; Tsai, Y. F.; Wanna, W. H.; Ramu, R.; Chan, S. I.; Zen, J. M.; Yu, S. S.-F. A Carbon Electrode Functionalized by a Tricopper Cluster Complex: Overcoming Overpotential and Production of Hydrogen Peroxide in the Oxygen Reduction Reaction. *Angew. Chemie - Int. Ed.* **2018**, *57*, 3612−3616.
(28) Taki, M.; Teramae, S.; Nagatomo, S.; Tachi, Y.; Kitagawa, T.; Itoh, S.; Fukuzumi, S. Fine-Tuning of Copper(I)-Dioxygen Reactivity by 2-(2-Pyridyl)Ethylamine Bidentate Ligands. *J. Am. Chem. Soc.* **2002**, *124*, 6367−6377.
(29) Cook, B. J.; Di Francesco, G. N.; Kieber-Emmons, M. T.; Murray, L. J. A Tricopper(I) Complex Competent for O Atom Transfer, C−H Bond Activation, and Multiple O_2 Activation Steps. *Inorg. Chem.* **2018**, *57*, 11361−11368.
(30) Lionetti, D.; Day, M. W.; Agapie, T. Metal-Templated Ligand Architectures for Trinuclear Chemistry: Tricopper Complexes and Their O_2 Reactivity. *Chem. Sci.* **2013**, *4*, 785−790.
(31) Engelmann, X.; Farquhar, E. R.; England, J.; Ray, K. Four-Electron Reduction of Dioxygen to Water by a Trinuclear Copper Complex. *Inorg. Chim. Acta* **2018**, *481*, 159−165.
(32) Tsui, E. Y.; Day, M. W.; Agapie, T. Trinucleating Copper: Synthesis and Magnetostructural Characterization of Complexes Supported by a Hexapyridyl 1,3,5-Triarylbenzene Ligand. *Angew. Chemie - Int. Ed.* **2011**, *50*, 1668−1672.
(33) Karlin, K. D.; Qingfen, G.; Farooq, A.; Shuncheng, L.; Zubieta, J. Synthesis and X-Ray Crystal Structure of a Trinuclear Copper(I) Cluster. *Inorg. Chim. Acta* **1989**, *165*, 37−39.
(34) Brown, E. C.; Johnson, B.; Palavicini, S.; Kucera, B. E.; Casella, L.; Tolman, W. B. Modular Syntheses of Multidentate Ligands with Variable N-Donors: Applications to Tri- and Tetracopper(i) Complexes. *J. Chem. Soc. Dalt. Trans.* **2007**, No. 28, 3035−3042.
(35) Reed, C. J.; Agapie, T. Thermodynamics of Proton and Electron Transfer in Tetranuclear Clusters with $Mn\text{-}OH_2/OH$ Motifs Relevant to H_2O Activation by the Oxygen Evolving Complex in Photosystem II. *J. Am. Chem. Soc.* **2018**, *140*, 10900−10908.
(36) Rhile, I. J.; Mayer, J. M. One-Electron Oxidation of a Hydrogen-Bonded Phenol Occurs by Concerted Proton-Coupled Electron Transfer. *J. Am. Chem. Soc.* **2004**, *126*, 12718−12719.
(37) Tyburski, R.; Liu, T.; Glover, S. D.; Hammarström, L. Proton-Coupled Electron Transfer Guidelines, Fair and Square. *J. Am. Chem. Soc.* **2021**, *143*, 560−576.
(38) Tian, S.; Jones, S. M.; Jose, A.; Solomon, E. I. Chloride Control of the Mechanism of Human Serum Ceruloplasmin (Cp) Catalysis. *J. Am. Chem. Soc.* **2019**, *141*, 10736−10743.
(39) Jung, J.; Kim, S.; Lee, Y. M.; Nam, W.; Fukuzumi, S. Switchover of the Mechanism between Electron Transfer and Hydrogen-Atom Transfer for a Protonated Manganese(IV)−Oxo Complex by Changing Only the Reaction Temperature. *Angew. Chemie - Int. Ed.* **2016**, *55*, 7450−7454.
(40) Morimoto, Y.; Park, J.; Suenobu, T.; Lee, Y. M.; Nam, W.; Fukuzumi, S. Mechanistic Borderline of One-Step Hydrogen Atom Transfer versus Stepwise Sc^{3+}-Coupled Electron Transfer from Benzyl Alcohol Derivatives to a Non-Heme Iron(IV)-Oxo Complex. *Inorg. Chem.* **2012**, *51*, 10025−10036.
(41) Usharani, D.; Lacy, D. C.; Borovik, A. S.; Shaik, S. Dichotomous Hydrogen Atom Transfer vs Proton-Coupled Electron Transfer during Activation of X-H Bonds (X = C, N, O) by Nonheme Iron-Oxo Complexes of Variable Basicity. *J. Am. Chem. Soc.* **2013**, *135*, 17090−17104.
(42) Bailey, W. D.; Dhar, D.; Cramblitt, A. C.; Tolman, W. B. Mechanistic Dichotomy in Proton-Coupled Electron-Transfer Reactions of Phenols with a Copper Superoxide Complex. *J. Am. Chem. Soc.* **2019**, *141*, 5470−5480.
(43) Shleev, S.; El Kasmi, A.; Ruzgas, T.; Gorton, L. Direct Heterogeneous Electron Transfer Reactions of Bilirubin Oxidase at a Spectrographic Graphite Electrode. *Electrochem. commun.* **2004**, *6*, 934−939.
(44) Kjaergaard, C. H.; Durand, F.; Tasca, F.; Qayyum, M. F.; Kauffmann, B.; Gounel, S.; Suraniti, E.; Hodgson, K. O.; Hedman, B.; Mano, N.; Solomon, E. I. Spectroscopic and Crystallographic Characterization of "Alternative Resting" and "Resting Oxidized" Enzyme Forms of Bilirubin Oxidase: Implications for Activity and Electrochemical Behavior of Multicopper Oxidases. *J. Am. Chem. Soc.* **2012**, *134*, 5548−5551.

https://doi.org/10.1021/jacs.1c10948
J. Am. Chem. Soc. 2022, 144, 1709−1717